Design and Evaluation of a Passive Alcove-Based Microfluidic Mixer

ARTICLE *in* ANALYTICAL CHEMISTRY · FEBRUARY 2009

Impact Factor: 5.64 · DOI: 10.1021/ac802410g · Source: PubMed

5 AUTHORS, INCLUDING:

Tsuyoshi Egawa
Yeshiva University
78 PUBLICATIONS **1,964** CITATIONS
SEE PROFILE

Eric Yale Hayden
University of California, Los Angeles
14 PUBLICATIONS **114** CITATIONS
SEE PROFILE

Published in final edited form as:
Anal Chem. 2009 February 15; 81(4): 1622–1627. doi:10.1021/ac802410g.

Design and Evaluation of a Passive Alcove-based Microfluidic Mixer

Tsuyoshi Egawa, **Jorge L. Durand**, **Eric Hayden**, **Denis L. Rousseau**[*], and **Syun-Ru Yeh**[*]
Department of Physiology and Biophysics, Albert Einstein College of Medicine, 1300 Morris Park Avenue, Bronx, NY 10461

Abstract

A novel passive microfluidic silicon mixer has been designed, optimized and fabricated. The architecture of the mixer consists of a simple "T" junction, made up by a 20 μm wide by 82 μm deep channel, followed by three repeats of an alcove, each with a triangular obstruction, arranged in a zigzag fashion. Numerical simulations were employed to optimize the geometry, particularly the dimensions of the alcoves, the relative orientation and the spacing between them, and the degree of intrusion associated with them. The simulation results demonstrate that chaotic flow due to recirculation within the alcoves results in transverse velocity that promotes effective fluid mixing. The microfluidic mixer with the simulation-optimized geometry was fabricated with photolithographic techniques and characterized by optical imaging, fluorescence and Raman microscope spectroscopy. At a sample flow rate of 20 μL/s, the mixer exhibits a short mixing deadtime of ~22 μs and a high mixing efficiency under both low and high viscosity conditions. The alcove-based microfluidic silicon mixer offers unique advantages for its short deadtime and slow sample consumption rate. In addition, it provides a valuable component for lab-on-a-chip applications for its ease of development into multiple networks for massively parallel analytical processes.

Introduction

Although mixing on a microscopic scale is a nontrivial task, the recent development of microfluidic solution mixers has allowed biological[1–5] and chemical reactions[6] to be measured on a time scale of less than 1 ms with relatively small sample volumes (for recent reviews, see refs[7–10]). Microfluidic mixers can be grouped into two categories, active and passive mixers, on the basis of the types of strategies employed to mix two solutions. Active mixers use an external field to generate turbulence that promotes mixing, whereas passive mixers do not use any external forces; instead, they rely on the geometry of the mixing chamber to introduce chaotic flow required for mixing.

In passive mixers, solution mixing depends on molecular diffusion, which is determined by the flow characteristics defined by the Reynolds number (*Re*). When a fluid flows through a pipe with a diameter of d, the Reynolds number can be calculated by the ratio of inertial forces ($v'\rho$) and viscous forces (μ/d):

$$Re=\frac{\rho v' d}{\mu} \qquad \text{Eq. 1}$$

[*]Corresponding authors: Syun-Ru Yeh, syeh@aecom.yu.edu, FAX: (718) 430–4230 Or Denis L. Rousseau, rousseau@aecom.yu.edu, FAX: (718) 430–8808.

where ρ μ and v' are the density, viscosity and linear flow rate of the fluid, respectively. Under conditions with low Reynolds numbers (*Re*<2,300), which is typical for microfluidic mixers, the flow is laminar and the mixing is limited by diffusion.[10] The diffusion time (τ_D) is δ^2/D, where δ is the diffusion length and D is the diffusion coefficient, which is ~10^{-9} m^2s^{-1} for small molecules in aqueous solvents. Thus, to achieve mixing in a sub-millisecond time window, the diffusion length has to be < 1 μm. On this basis, ingenious hydrodynamic focusing protocols, taking advantage of laminar flow conditions, instead of avoiding them, have been developed.[3, 11–14] With the hydrodynamic focusing method, a central stream is narrowed by bordering streams to a sub-micrometer dimension, such that mixing can occur within a submillisecond time window via diffusion processes. Likewise, splitting and subsequent rejoining the laminar streams via parallel[15] or serial[16] lamination paths have been designed to promote fluid mixing.

On the other hand, to overcome the limitations set by the diffusion processes, several novel microfluidic mixers have been designed to generate chaotic advection, in which a transversal component of the velocity is produced to facilitate mixing under conditions with a low Reynolds number (*Re*<2000).[1, 4, 5, 7–10, 16–21] Chaotic advection can be achieved by placing obstacles in the flow path,[4, 19, 21, 22] by building ribs, grooves or other structures on the bases or walls of the flow channels,[23–25] or by simply modulating flow channel geometries in a zigzag fashion, following a T- or Y-junction.[18] It can also be accomplished by modulating the shape of the two inlets, prior to a T- or Y-junction, thereby disturbing the laminar flow of the fluids prior to their entry into the junction.[5]

In a previous report,[4] we described a unique microfluidic mixer, in which the two fluid streams to be mixed were introduced head-to-head into a 450 pL mixing chamber containing seven vertical pillars to introduce turbulence, thereby ensuring rapid and efficient mixing. With an output velocity of 20 μl/s, the deadtime was determined to be 50 μs. Although the mixing efficiency is satisfactory for typical aqueous solutions, it is significantly diminished for mixing under high viscosity conditions, which is often required for biological reactions. To improve the mixing efficiency under extreme conditions, we sought to design a new passive chaotic microfluidic mixer based on a modified flow channel with ‘recirculating’ alcoves attached to it in a zigzag fashion. Using computer simulations, we have optimized the geometry of the mixer. We show that, with a sample consumption rate of 20 μl/s, reliable mixing can be achieved within 22 μs under conditions with a Reynolds number <400 in both high and low viscosity solvents.

Methods

Computational Analysis

All the simulations were carried out by using the open source multiphysical simulation software, Elmer, which was developed by the Finnish IT Center for Science (CSC) and is available through their web site, http://www.csc.fi/elmer/ With this software, two-dimensional numerical solutions of the static Navier-Stokes equation were obtained. Fluid velocity vectors were generated as node points of a 3 μm-size triangle mesh grid based on finite element simulations. The initial fluid flow velocity (v_0) at the inlet was set to be 20 m/s and zero along the vertical (v_y) and horizontal (v_x) axes, respectively. For positions along the wall surface, both the vx and vy were set to be zero; in contrast, no boundary restriction was applied to the outlet. The density (ρ) and viscosity (μ) of fluid material were set at 10^3 kg/m^3 and 10^{-3} kg/m/s, respectively, based on the parameters of water at 20°C.

Fabrication and Experimental Characterization

The silicon mixer was fabricated at the Stanford Nanofabrication Facility, based on procedures described previously.[4] Optical and fluorescence imaging, as well as Raman measurements, were carried out with a LabRam HR microscopy system from HORIBA Jobin Yvon (Edison, NJ) equipped with a motorized microscope stage (EK32 75×50 from Märzhäuser, Wetzlar-Steindorf, Germany). Raman scattering was excited at 784.7 nm by a XTRA diode laser from Topica Photonics Inc. (Victor, NY). The fluorescence images were obtained by mixing fluorescein with a fluorescence quencher, sodium iodide (500 mM). The two solutions in 100 mM sodium phosphate buffer (pH 7.0) were loaded into two separate syringes and delivered into the mixers by a syringe pump. The concentration of fluorescein used for the global imaging and point-by-point scanning modes are 11.4 mM and 30 μM (before the mixing), respectively. For the global fluorescence imaging measurements, fluorescein was excited with white light from a xenon lamp (Euromex, Holland), while for the point-by-point scanning fluorescence measurements, fluorescein was excited at 441.6 nm from a helium-cadmium laser from Kimmon Electric US (Centennial, CO). Fluorescein was purchased from Eastman Organic Chemicals (Rochester, NY), and the other chemicals were purchased from Sigma Chemical Co. (St. Louis, MO).

Results and Discussion

A series of microfluidic silicon mixers were designed and fabricated by using standard photolithographic techniques in the Stanford Nanofabrication Facility. All the features were etched into the silicon substrate with an anisotropic etching method, which resulted in rectangular-shaped channels with flat bottoms. The fabricated silicon chip was enclosed by a glass window with two through-holes matching the two entrances of the “T” junction on the silicon by an anodic bonding method.[4] The mixers were tested by fluorescence imaging obtained by mixing equal volumes of fluorescein and sodium iodide, a dynamic quencher of fluorescein with a flow speed of 20 μl/s. Among these mixers, the one that displayed the best performance has an architecture with alcoves connected in a zigzag fashion (Fig. 1A). Similar zigzag features without alcoves have been shown to induce chaotic advection in microfluidic mixers.[18, 20] As shown in Fig. 1B, the fluorescence imaging data indicate that almost no apparent mixing occurred in the first mixing alcove labeled as (i), where the two solutions first encounter each other. On the other hand, significant mixing was observed and gradually improved as the solution mixture traveled down the three subsequent alcoves. Additional measurements with high viscosity solvents show similar mixing efficiency, demonstrating the usefulness of this mixer. In an effort to optimize the design of the mixer, the self-circulation of fluid introduced by the alcoves attached to a flow channel was simulated as a function of various parameters as described below.

Computer Simulations

For the simulations, the initial linear velocity (v_0) was set at 20 m/s at the inlet of the flow channel with a width (L) of 20 μm. It corresponds to a sample consumption rate of 20 μl/s, with a channel depth of 100 μm. The density, ρ and viscosity, μ are set at 10^3 kg/m^3 and 10^{-3} kg/m/s, respectively.

As a first series of simulations, the fluid dynamics in an alcove attached to a linear flow passage was monitored by varying one dimension of the rectangular alcove, defined as M in Fig. 2, from 0.5 L to 2.5 L, while the other dimension was kept constant at 2.0 L. As shown on the top, the attachment of the alcove to the flow channel introduces significant recirculation of fluid. The blow-up view of the alcove is shown at the bottom of each design for clarity. The data show that the degree of recirculation within the alcove increases as M increases from 0.5 to 1.5 L, while further increase in M to 2.5 L introduces a dead-space in

the far corners of the alcove, where the fluid velocity is essentially zero, which is detrimental for mixing. Accordingly, we conclude that the optimum size of the alcove is M=1.5 L.

Although the presence of a simple alcove generates recirculation flow, which is expected to create a vortex that is advantageous for fluid mixing, in most applications the two solutions to be mixed enter the flow channel in a laminar fashion and only the solution that enters on the alcove side would be disturbed. As such, the recirculation flow in the alcove would not be sufficient to promote complete mixing of two solutions, especially under the conditions with a low Reynolds number. To overcome this problem, we sought to add a triangular obstruction on the alcoves, as shown in Fig. 3, to direct the second solution into the recirculation alcove dominated by the first solution. To simulate the fluid dynamics in the new mixer, we fixed the value of M at 1.5 L, and varied the size of the triangular obstruction, defined by N in Fig. 3, from 0.25 L to 1.75 L. It was found that, when N=0.25 L, the solution is hardly disturbed (data not shown). But, as N was gradually increased to 0.75–1.25 L, the chaotic recirculation flow goes deeper into the alcove. Further increase of N to 1.75 L caused a reduction of the recirculation vortex (see the blow-up views in the bottom of Fig. 3). Consequently, we conclude that the best value of N lies in the 0.75 – 1.25 L range.

In the last series of simulations, the relative arrangement of three repeats of the alcove containing the triangular obstruction was varied and examined. The M and N parameters were fixed at 1.5 and 1.25 L, respectively. We first compared two mixers, one with all three alcoves on the same side and the other with them positioned in a zigzag fashion, as shown in Fig. 4A–B. The simulation results show significant enhancement in the recirculation in the second and third alcoves in the zigzag mixer. To further improve fluid recirculation, mixers with three alcoves arranged in a zigzag pattern were evaluated as a function of their spacing defined as S in Fig. 4. The data show that the recirculation vortex was slightly reduced when the separation between the alcoves was reduced from 1.0 L (B) to zero (C). But as the separation was further reduced to a degree such that the alcoves overlap with each other (D), a dramatic reduction in the recirculation vortex was observed. On the other hand, a further increase of the separation to > 1.0 L did not affect the recirculation vortex (data not shown). As an increase in the spacing is expected to increase the deadtime of the mixer, which is disadvantageous for rapid mixing applications, we concluded that the optimized separation between the alcoves lies at 0 L.

Design of a new Microfluidic Silicon Mixer

Taken together the simulation data demonstrate that the addition of alcoves attached to a flow channel can induce flow velocity vectors transverse to the overall flow direction, and that the resulting chaotic advection[18, 20] is expected to promote chaotic mixing of fluids.[10] On the basis of the simulation-optimized parameters, we have constructed a new microfluidic mixer, in which M and N were set to be 1.5 and 1.0 L, and the spacing between the alcoves (S) was fixed to be zero. As the data obtained from the preliminary design (Fig. 1) show that the alcove (i) connecting the two solution inlets did not appear to establish mixing, a simple T mixing junction was used to introduce the two solutions together prior to their merging in the mixing chamber.

As shown in Fig. 5A, in the new mixer, the two solutions to be mixed enter at opposite sides of the 20 μm channel and meet at the central “T” junction, where they are directed into a 20 μm channel with the three alcoves attached to it in a zigzag fashion. The mixed solution exits from a 120 μm long channel with a width of 20 μm as a free solution jet. All the features were etched into the silicon substrate, to a depth of 82 μm, with an isotropic etching method. As the T-junction did not introduce mixing (see discussion below), the time zero

was assigned to be at the entrance of the first mixing alcove. The reaction times at the various positions are indicated in Fig. 5A, as calculated based on the physical size of the features, as well as a flow rate of 20 μl/s.

Performance of the New Microfluidic Mixer

To characterize the new mixer shown in Fig. 5, we first used a fluorescence imaging method to view the flow dynamics, following the mixing of fluorescein and sodium iodide (a dynamic quencher of fluorescein). With 500 mM sodium iodide applied, ~70% quenching of the fluorescence from fluorescein is expected upon complete mixing.[26] As shown in Fig. 5B, the two solutions exit the T junction in a laminar regime without observable mixing between them. Nonetheless, the color distribution becomes more and more homogeneous as the solutions pass down the three alcoves. At the end of the last alcove, a completely homogeneous color was observed, indicating complete mixing of the two solutions.

To further evaluate the mixing efficiency in a quantitative fashion, Raman spectroscopy was employed to monitor a pH jump reaction of a phosphate buffer. In this reaction, a mono-basic sodium phosphate (NaH_2PO_4) solution (0.625M, pH 4.4), was mixed with an equal volume of a Tris buffer (0.417M, pH 10.5) to induce the deprotonation of $H_2PO_4^-$ to HPO_4^{2-}, which have characteristic Raman lines at 877 and 990 cm^{-1}, respectively (see the inset in Fig 6B). The mixed free solution jet at the exit of the mixer was probed by a laser beam focused on the jet by an objective lens of a Raman microscope system. The scattered light was collected by the same lens, in a back-scattering geometry, and directed into a spectrometer system for spectral analysis. With this system the laser beam can be focused to a small spot, with a diameter of a few microns, allowing the examination of the cross-section of the jet from P1, P2 to P3, as indicated in the microscope image of the jet shown in Fig. 6C. At a final flow rate of 20 μL/s, the mixed solution exits from the silicon mixer as a free solution jet with a diameter of ~50 μm.

As shown in Fig. 6A, the spectra obtained at P_1, P_2 and P_3 are essentially identical, as highlighted in the P_3-P_1 and P_3-P_2 difference spectra, confirming the solution jet is homogeneous in the plane perpendicular to the flow direction. To quantify the mixing efficiency, the spectrum obtained at position P_3 was compared with those of various equilibrium mixtures of NaH_2PO_4 and pH 10.5 Tris buffer solutions. The data indicate that the spectrum of an equal volume mixture is almost identical to the P_3 spectrum (see the top blue and black traces in Fig. 6B, respectively, as well as the difference spectrum between them shown at the bottom), whereas a volume ratio of 0.525:0.475 leads to a slightly higher peak intensity at 877 cm^{-1} (the magenta spectrum) as compared to the P_3 spectrum. The data indicate complete mixing of the two solutions at the outlet of the new microfluidic mixer.

To confirm that the T-junction in the mixer does not contribute to the mixing of the two solutions, a simple T mixer identical to that shown in Fig. 5A, with all the alcoves eliminated, was fabricated. The NaH_2PO_4 and Tris solutions were introduced from the P_1 and P_3 sides of the T junction in the mixer, respectively, at a final flow rate of 20 μL/s. The Raman spectra were obtained at positions P_1, P_2 and P_3 in the free solution jet as described above. As shown at the bottom of Fig. 6A, the Raman spectrum obtained at the P_1 position is essentially the same as that of the pure NaH_2PO_4 solution, whereas that obtained at the P_3 position shows no Raman signal (data not shown), consistent with that of the pH 10.5 Tris buffer. The data confirm that no mixing occurred in the T junction and that the two solution streams exit the T mixer in a laminar fashion. On the basis of these data, we conclude that the efficient mixing observed in the mixer shown in Fig. 5 is mainly a result of the recirculation flow generated in the alcoves arranged in the zigzag pattern.

Although the Raman measurements gave an excellent quantitative measure of the mixing efficiency at the output of the jet, it is not easy to obtain the spectra of $H_2PO_4^-/HPO_4^{2-}$ in the mixing chamber of the mixer due to the intrinsic weakness of the band intensities. To investigate how the two solutions are mixed in the mixing chamber in a quantitative fashion, a series fluorescence spectra was obtained following the initiation of the mixing of fluorescein with sodium iodide, via point-by-point scanning over the entire mixer by using the 441.6 nm output from a helium-cadmium laser. The x–y positioning of the mixer was controlled by a precision motorized stage, with a 0.1 μm spatial resolution. The focal plane along the z axis was set at 20 μm from the interface between the silicon and glass cover of the mixer. The spatial resolution of the image on the x–y plane and along the z-axis are ~3 and 20 μm, respectively, as controlled by the microscope objective lens employed (50× LMPlanFl Olympus with 0.50 NA and 10.6 mm working distance). The spectrum at every given position was corrected by subtracting the background spectrum, obtained at the same position with only the buffer solution flowing through the mixer, from it. The equilibrium fluorescence spectrum of the completely mixed solution was obtained as a reference. In Fig. 7B, three representative fluorescence spectra, at positions (i), (ii) and (iii) are shown compared to the reference spectrum. As the fluorescein and iodide solutions entered from the right and left sides of the entrance channel in a laminar fashion (see Fig. 5B), the fluorescence intensity obtained in the alcove on the right side of the channel (i) is stronger than the reference, whereas that on the left side of the channel (ii) is weaker than the reference; it becomes identical to the reference as the flow reaches the position (iii), indicating the complete mixing of the solutions, consistent with the Raman data shown in Fig. 6.

The mixing efficiency at every given position can be calculated according to the following equation.[7–10]

$$Mixing\ Efficiency\ (\%) = \left\{1 - \sqrt{\left(\frac{I_s - I_{ref}}{I_{ref}}\right)^2}\right\} \times 100$$

Where I_s and I_{ref} stand for the integrated fluorescence intensities in the 500–700 nm window of the sample and reference, respectively. The color coded mixing efficiency map of the mixer shown in Fig. 7A was constructed based on the mixing efficiencies thus calculated. The data are qualitative correlated with the simulation data shown in Fig. 4C, confirming the reliability of our simulation data. It is noted that the occasional small areas with high mixing efficiencies at the beginning of the mixer are a consequence of the chaotic flow resulting from recirculation introduced by the alcove structures.

To further examine the performance of the mixer under high viscosity conditions, we repeated the same fluorescence measurements by including 1, 2 or 3 M guanidine in the fluorescein and iodide solutions to be mixed. The viscosities of the solutions relative to that of pure water are 1.038, 1.095 and 1.170, respectively.[27] As summarized in Table I, the mixing efficiencies obtained at the position (iii), decrease from 99, 97 to 90%, as the guanidine concentration increasing from 1, 2 to 3 M, respectively. They are associated with a slightly increasing degree of fluctuation in the fluorescence intensity, from 2.7, 3.0 to 4.9 %, respectively, suggesting that the solutions were not mixed perfectly at microscopic level in the high viscosity solvents. The fluctuations plausibly result from microscopic clusters of partially mixed solutions produced during mixing under the high viscosity conditions. Nonetheless, according to the data, 90% mixing efficiency was achievable with a solution viscosity of 1.170.

Conclusions

To study rapid biochemical and chemical reactions, solution mixers with small sample consumption rates and high mixing efficiencies, under both low and high viscosity conditions, are valuable. Here, the novel design of a passive microfluidic mixer, which is readily fabricated by standard photolithographic techniques, is presented. In this mixer, three repeats of a recirculation alcove with a triangular obstruction are attached to the flow channel in a zigzag fashion. Computer simulations demonstrate that when the dimensions of the alcoves and the obstructions, as well as the relative orientation of the alcoves and spacing between them, are optimized, chaotic advection promoting efficient fluid mixing is induced. By using Raman and fluorescence spectroscopies, the mixing was determined to be nearly complete under both high and low viscosity conditions, at a flow velocity of 20 μL/s. Under these flow conditions, the deadtime was determined to be ~22 μs. With this mixer, the progression of a reaction following mixing can be probed spectroscopically in real time on the mixer chip or on the output free solution jet exiting from the mixer. Alternatively, the reaction intermediates may be trapped by directing the solution jet to a freeze–quenching device such as a home-made double-wheel apparatus,[4, 28] or into a isopentane bath at various reaction times for later characterization. The simple design and excellent performance of this mixer opens a new window for handling complex biochemical and chemical reactions in parallel analytical processes on a single silicon substrate, realizing Lab-on-a-Chip applications.

Acknowledgments

We would like to thank Dr. Mary Tang for assistance in the fabrication of the silicon mixers. SRY and DLR would like to acknowledge a CIS user grant from the Stanford Nanofabrication Facility and NIH (GM054806 and GM074982), respectively, for support of this work.

References

1. Takahashi S, Yeh SR, Das TK, Chan CK, Gottfried DS, Rousseau DL. Nat Struct Biol. 1997; 4:44–50. [PubMed: 8989323]
2. Yeh SR, Han SW, Rousseau DL. Accounts of Chemical Research. 1998; 31:727–736.
3. Kauffmann E, Darnton NC, Austin RH, Batt C, Gerwert K. Proceedings of the National Academy of Sciences of the United States of America. 2001; 98:6646–6649. [PubMed: 11371608]
4. Lin Y, Gerfen GJ, Rousseau DL, Yeh SR. Anal Chem. 2003; 75:5381–5386. [PubMed: 14710815]
5. Matsumoto S, Yane A, Nakashima S, Hashida M, Fujita M, Goto Y, Takahashi S. J Am Chem Soc. 2007; 129:3840–3841. [PubMed: 17375918]
6. deMello AJ. Nature. 2006; 442:394–402. [PubMed: 16871207]
7. Ottino JM, Wiggins S. Philosophical Transactions of the Royal Society of London Series a-Mathematical Physical and Engineering Sciences. 2004; 362:923–935.
8. Campbell CJ, Grzybowski BA. Philosophical Transactions of the Royal Society of London Series a-Mathematical Physical and Engineering Sciences. 2004; 362:1069–1086.
9. Ottino JM, Wiggins S. Science. 2004; 305:485–486. [PubMed: 15273385]
10. Nguyen NT, Wu ZG. Journal of Micromechanics and Microengineering. 2005; 15:R1–R16.
11. Knight JB, Vishwanath A, Brody JP, Austin RH. Physical Review Letters. 1998; 80:3863–3866.
12. Park HY, Qiu X, Rhoades E, Korlach J, Kwok LW, Zipfel WR, Webb WW, Pollack L. Anal Chem. 2006; 78:4465–4473. [PubMed: 16808455]
13. Hertzog DE, Ivorra B, Mohammadi B, Bakajin O, Santiago JG. Anal Chem. 2006; 78:4299–4306. [PubMed: 16808436]
14. Yao S, Bakajin O. Anal Chem. 2007; 79:5753–5759. [PubMed: 17583912]
15. He B, Burke BJ, Zhang X, Zhang R, Regnier FE. Analytical Chemistry. 2001; 73:1942–1947. [PubMed: 11354474]

16. Munson MS, Yager P. Analytica Chimica Acta. 2004; 507:63–71.
17. Groisman A, Steinberg V. Nature. 2001; 410:905–908. [PubMed: 11309609]
18. Mengeaud V, Josserand J, Girault HH. Analytical Chemistry. 2002; 74:4279–4286. [PubMed: 12199603]
19. Wang HZ, Iovenitti P, Harvey E, Masood S. Smart Materials & Structures. 2002; 11:662–667.
20. Stremler MA, Haselton FR, Aref H. Philosophical Transactions of the Royal Society of London Series a-Mathematical Physical and Engineering Sciences. 2004; 362:1019–1036.
21. Wang RJ, Lin JZ, Li HJ. Chaos Solitons & Fractals. 2007; 33:1362–1366.
22. Bhagat AAS, Peterson ETK, Papautsky I. Journal of Micromechanics and Microengineering. 2007; 17:1017–1024.
23. Johnson TJ, Ross D, Locascio LE. Anal Chem. 2002; 74:45–51. [PubMed: 11795815]
24. Stroock AD, Dertinger SK, Whitesides GM, Ajdari A. Anal Chem. 2002; 74:5306–5312. [PubMed: 12403585]
25. Stroock AD, Dertinger SK, Ajdari A, Mezic I, Stone HA, Whitesides GM. Science. 2002; 295:647–651. [PubMed: 11809963]
26. Albani JR. Biochim Biophys Acta. 1998; 1425:405–410. [PubMed: 9795256]
27. Kawahara K, Tanford C. J Biol Chem. 1966; 241:3228–3232. [PubMed: 5912116]
28. Tanaka M, Matsuura K, Yoshioka S, Takahashi S, Ishimori K, Hori H, Morishima I. Biophys J. 2003; 84:1998–2004. [PubMed: 12609902]

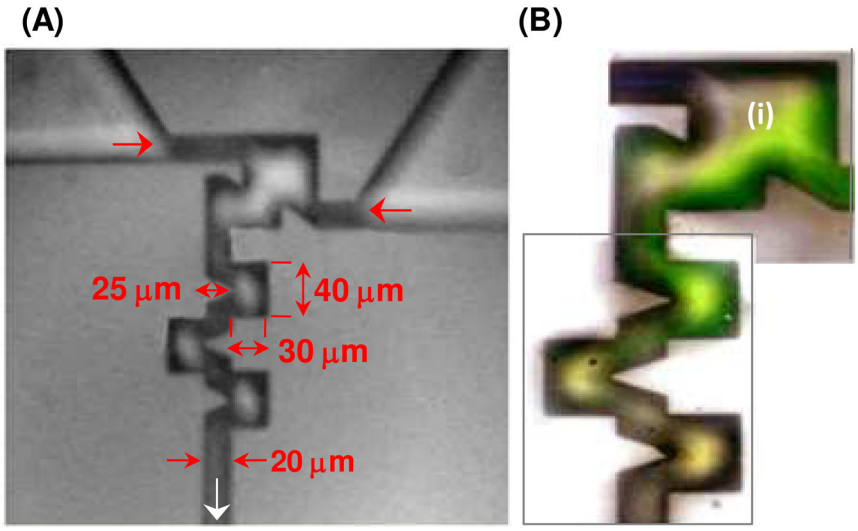

Fig. 1. The optical (A) and fluorescence (B) image of the mixing chamber of a novel silicon microfluidic mixer

The dimensions of the mixer are as indicated in (A). The fluorescence image (B) was obtained by mixing equal volumes of 11.4 mM fluorescein with 500 mM sodium iodide at a final flow rate of 20 μL/s.

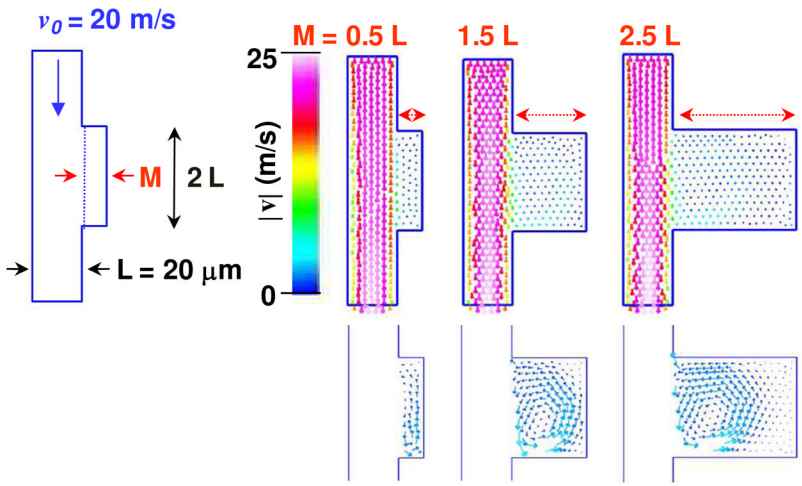

Fig. 2. Velocity vectors describing the flow recirculation induced by an alcove attached to a linear flow passage as a function of the aspect ratio M/L

The parameters M and L are as defined in the cartoon shown on the left. The arrows represent the velocity vectors of the fluid flow. The amplitudes of the velocity vectors are color coded from blue to white as indicated by the velocity scale; within each color, the amplitudes are represented by the lengths of the arrows. In the bottom images, only velocity vectors within 15 % of the maximum velocity are shown; for clarity the vectors are scaled up by a factor of 10 with respect to those shown in the top images.

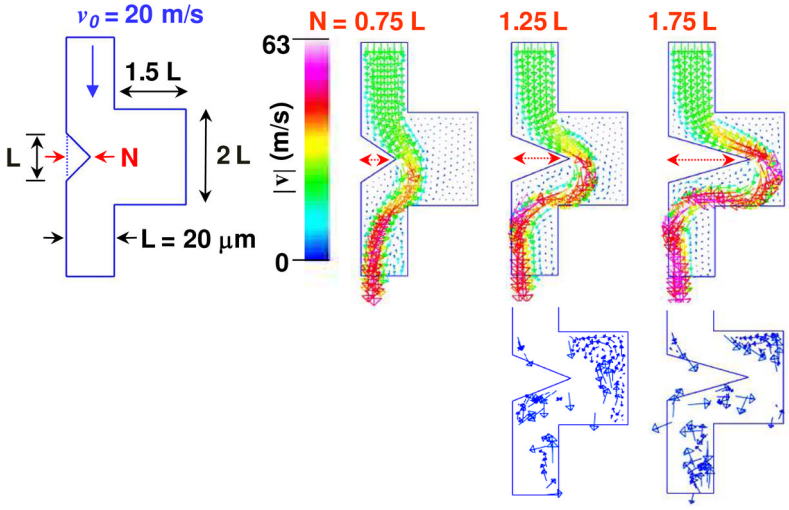

Fig. 3. Velocity vectors describing the flow recirculation induced by an alcove with a triangular obstruction as a function of the size of the obstruction defined by N

The representations for the velocity vectors are the same as those defined in Fig. 2. In the bottom images, only velocity vectors within 6 % of the maximum velocity are shown; for clarity the vectors are scaled up by a factor of 10 with respect to those shown in the top images.

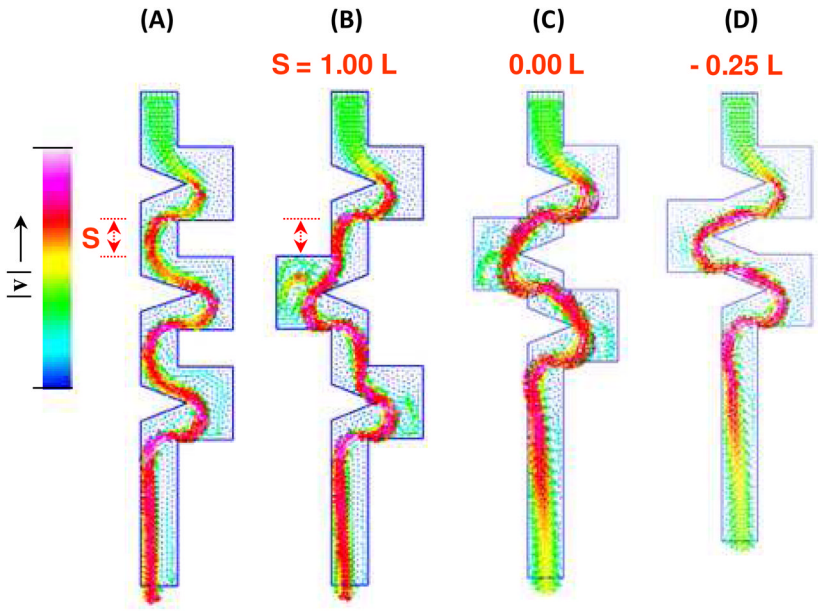

Fig. 4. Velocity vectors describing the flow recirculation in three repeats of an alcove, with a triangular obstruction, as a function of their relative positioning

The representations for the velocity vectors are the same as those defined in Fig. 2, except that the colors are independently normalized for each design on the basis of the maximum velocity. The maximum velocities in the designs (A)–(D) were 68, 61, 56, and 63 m/s, respectively.

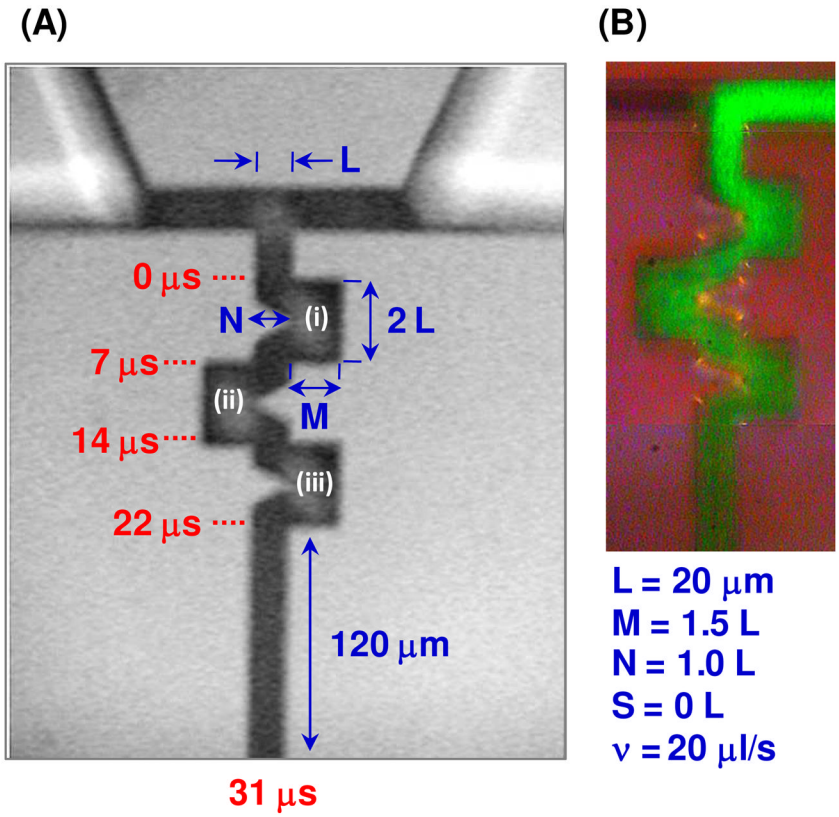

Fig. 5. The optical (A) and fluorescence (B) image of the mixing chamber of the new alcove-based microfluidic mixer

The dimensions of the features in the mixer are as indicated in blue in (A). The depth of the flow passage is 82 μm. The red numbers indicate the calculated reaction time at each position, with a flow rate of 20 μL/s. In (B), 11.4 mM of fluorescein was mixed with equal volume of 500 mM sodium iodide at a final flow rate of 20 μL/s. The data was obtained by global imaging of the fluorescence from fluorescein, exited by a Xe lamp.

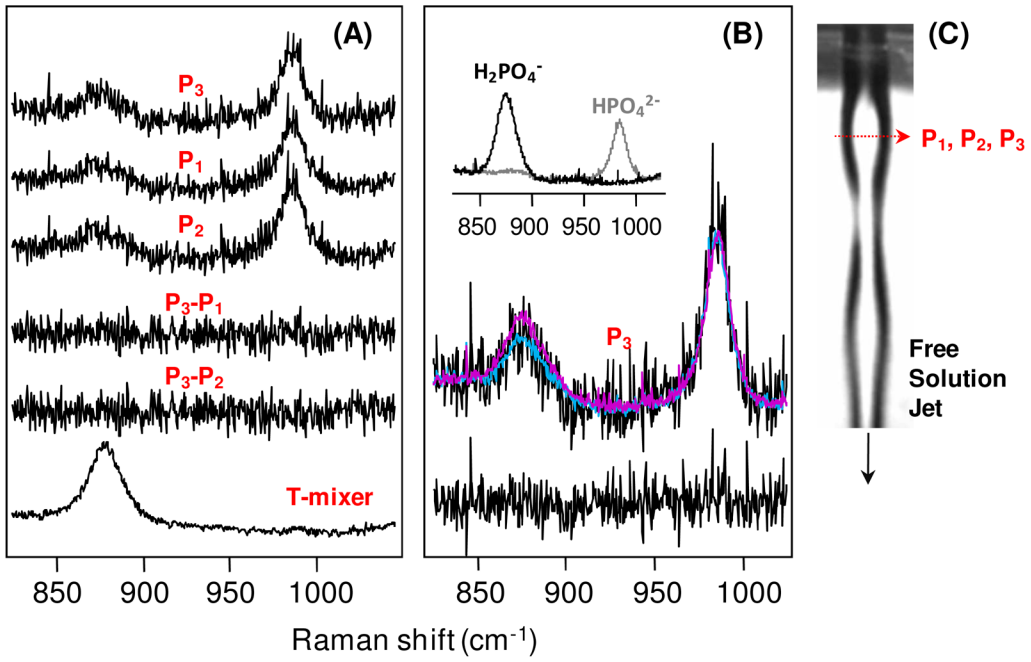

Fig. 6. The evaluation of the mixing efficiency of the microfluidic mixer by using Raman spectroscopy (A–B) and the optical image of the free solution jet exiting from the alcove-based microfluidic mixer (C)

The Raman spectra in (A–B) were obtained ~300 μm downstream from the exit of the jet at three positions, P_1, P_2 and P_3, as indicated in (C), following the mixing of equal volumes of NaH_2PO_4 (0.625 M) and pH 10.5 Tris buffer (0.417 M) solutions at a flow rate of 20 μL/s. The laser beam for Raman excitation was focused to <2 μm spot by using a microscope objective lens. The dimension of the free solution jet is ~80 μm. The P_2 position was in the center of the jet, whereas the P_1 and P_3 positions were ~30 μm away from the center. The P_3-P_1 and P_3-P_2 difference spectra are as indicated. The bottom spectrum was obtained from a simple T mixer under the same mixing condition as a reference (the spectrum was obtained slightly off the center of jet towards the NaH_2PO_4 side). The top spectra in (B) show the comparison between the Raman spectrum obtained at position P_3 (black) and those of the equilibrium mixture of NaH_2PO_4 (0.625 M) and pH 10.5 Tris buffer (0.417 M) at a volume ratio of 0.525:0.475 (magenta) and 0.5:0.5 (blue). The bottom trace is the difference spectrum between the black and blue traces. The inset in (B) shows the Raman spectra of the equilibrium mixture of 0.625 M NaH_2PO_4 and 0.417 M pH 10.5 Tris buffer solutions with a volume ratio of 1:0 (black) and 0.4:0.6 (gray).

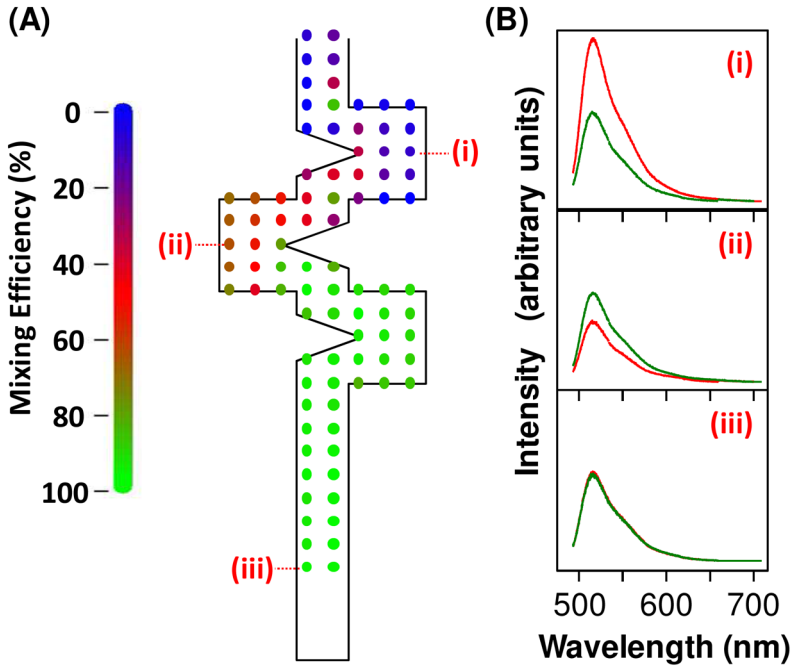

Fig. 7. Mixing efficiency map of the alcove-based microfluidic mixer

The mixing efficiency map in (A) was obtained by point-by-point scanning of the entire mixing chamber of the mixer mounted on a motorized x–y microscope stage as described in the text. The degree of mixing efficiency at a given position is color-coded base on the scale bar shown on the left. The representative background-corrected fluorescence spectra colored in red at three given position, as indicated, are shown in (B). The equilibrium spectrum colored in green, shown as a reference, represents the spectrum of the completely mixed solution. The fluorescence spectra were obtained with an excitation wavelength at 441.6 nm, an output from a helium-cadmium laser. The laser power was ~0.2 mW; the spectral acquisition time for each spectrum was 1 s. The solution and flow conditions of the mixing experiment are the same as those described in Fig. 5, except that the fluorescein concentration was reduced to 30 μM (before the mixing).

Table I

Mixing efficiency as a function of the Guanidine concentration

[Guanidine]	Relative Viscosity[a)]	Mixing Efficiency[b)]	Fluctuation[c)]
1 M	1.038	99 %	2.7 %
2 M	1.095	97 %	3.0 %
3 M	1.170	90 %	4.9 %

a) Viscosity relative to that of pure water.[27]

b) The mixing efficiencies were determined by the same method as that described for Fig 7.

c) The amplitudes of fluctuation were determined by a standard deviation analysis of 20 one, second fluorescence intensity measurements.